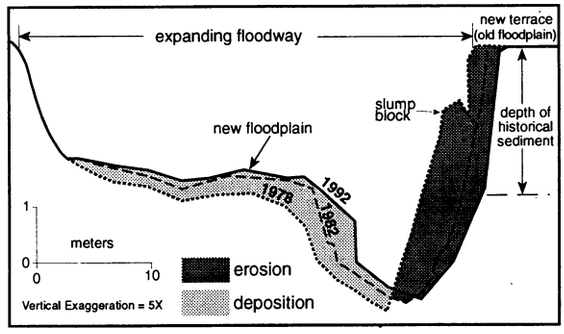

Fig. 3. A sediment source. This is a cross-sectional profile in the upper main valley of Coon Creek showing the removal of mostly historical sediment in a cut bank and the lateral expansion and accretion of a new, lower floodplain ~2 m below the level of the historical floodplain, now a terrace. As the channel has migrated laterally to the right over the past 60 years, the void between the levels of the new and old floodplains is indicative of the volume of sediment supplied downstream by this reach. A typical tributary cross section would be similar except the banks would be lower (1 to 2 m high) and deposition generally would be greater than erosion for the period 1975–93. [Modified from (9)]

that this is not the case. Other studies have also shown a decrease of sediment accretion rates in the Driftless Area over recent decades (*2, 3, 10, 14*).

Sediment sources, sinks, and fluxes for a stream basin are highly variable in space and time. Alluvial sediment storage has been greatly reduced in the Coon Creek Basin, but sediment yield from the basin has remained constant, further demonstrating the limited short-term diagnostic utility of sediment yields (*6*). Within the basin, sediment accretion rates in the lower main valley were only ~3 to 4% of the 1930s rates, but during the same period, the upper main valley has become a net sediment source and tributaries have been transformed from sediment sources to sinks. These distributed processes indicate the complex and variable quality of sediment sources and sinks within a basin, a principle first proposed by Brune in 1950 (*15*), which is exceedingly difficult to measure. General and substantial increases of soil erosion in the United States are not borne out by measurements of sedimentation in Coon Creek. The processes occurring in Coon Creek are indicative of many agriculturally disturbed basins in the eastern United States and elsewhere.

References and Notes

1. W. Dietrich and T. Dunne, *Z. Geomorphol. Suppl.* **29**, 191 (1978); H. Kelsey, *Geol. Soc. Am. Bull.* **91**, 190 (1980); F. Swanson, F. Janda, T. Dunne, D. Swanston, Eds., *Sediment Budgets and Routing in Forested Drainage Basins* (U.S. Department of Agriculture, Forest Service General Technical Report PNW141, 1982); R. Meade, *J. Geol.* **90**, 235 (1982); D. Walling, *J. Hydrol.* **65**, 209 (1983); P. Patton and P. Boison, *Geol. Soc. Am. Bull.* **97**, 369 (1986); J. Phillips, *Am. J. Sci.* **287**, 780 (1987); M. Church and O. Slaymaker, *Nature* **337**, 352 (1989); P. Ashmore, *Prog. Phys. Geogr.* **17**, 190 (1993); A. Schick and J. LeKach, *Phys. Geogr.* **14**, 225 (1993); O. Slaymaker, *ibid.*, p. 305; S. Trimble, in *Changing River Channels*, A. Gurnell and G. Petts, Eds. (Wiley, Chichester, UK, 1995), pp. 201–215; *Science* **278**, 1442 (1997).
2. S. Trimble, in *Landscapes of Wisconsin*, B. Zakrzewska-Borowiecki, Ed. (Association of American Geographers, Washington, DC, 1975), pp. 24–29; in *Proceedings of the Third Federal Interagency Sedimentation Conference* (Water Resources Council, Washington, DC, 1976), section 5, pp. 100–112.
3. ———, *Science* **214**, 181 (1981); S. Trimble and S. Lund, *U.S. Geol. Surv. Prof. Pap. 1234* (1982).
4. S. Trimble, *Am J. Sci.* **283**, 454 (1983).
5. W. Gebert and W. Krug, *J. Am. Water Resour. Assoc.* **32**, 733 (1996).
6. S. Trimble, *Science* **188**, 1207 (1975); *ibid.* **191**, 871 (1976); *Am. J. Sci.* **277**, 876 (1977).
7. ———, *Geology* **25**, 467 (1997).
8. ———, *Environ. Geol.* **32**, 230 (1997).
9. ———, *Phys. Geogr.* **14**, 285 (1993).
10. J. Knox, *Ann. Assoc. Am. Geogr.* **67**, 323 (1977); F. Magilligan, *ibid.* **75**, 583 (1985).
11. K. Potter, *Water Resour. Res.* **27**, 845 (1991); W. Krug, *J. Am. Water Resour. Assoc.* **32**, 745 (1996).
12. F. Steiner, *Soil Conservation in the United States: Policy and Planning* (Johns Hopkins Univ. Press, Baltimore, 1990); D. Pimentel *et al.*, *Science* **267**, 1117 (1995).
13. O. Owen, D. Chrias, J. Reganold, *Natural Resource Conservation* (Prentice Hall, Upper Saddle River, NJ, 1998).
14. J. Knox, *Ann. Assoc. Am. Geogr.* **77**, 224 (1987); T. Beach, *ibid.* **84**, 5 (1994).
15. G. Brune, *Trans. Am. Geophys. Union* **31**, 587 (1950).

16. This study was established in 1938 by the late S. C. Happ and the late V. E. McKelvey, and I am grateful for their gracious assistance. The study was supported by the U.S. Geological Survey, the Wisconsin Department of Natural Resources, the Natural Resources Conservation Service, the National Geographic Society, the NSF, the Wisconsin Department of Transportation, the University of California at Los Angeles Faculty Senate, and New Badger Enterprises. R. H. Meade designed Fig. 1. The report was greatly improved through critical reviews by M. Church, W. W. Emmett, A. Mendel, R. Shreve, L. Smith, and M. G. Wolman, but any errors remain mine. I also thank E. Brick and the many others who assisted me in the field.

18 May 1999; accepted 15 July 1999

Switchable Tackiness and Wettability of a Liquid Crystalline Polymer

Guillaume de Crevoisier,[1] Pascale Fabre,[1] Jean-Marc Corpart,[2] Ludwik Leibler[1]

The spreading velocity of liquids on the surface of a liquid crystalline polymer can be tremendously affected by a slight temperature change. Indeed, a bulk transition between a highly ordered smectic and an isotropic phase induces a sharp change from a rigid to a soft behavior, with consequent effects on the tack properties of the liquid crystalline polymer and on the dewetting dynamics of a liquid on its surface.

In many applications, it is desirable to control both the wetting and adhesive properties of a surface. Wettability reflects whether a liquid will spread on a surface as a continuous film or, conversely, retract as one or several droplets. There are many ways to control the wettability of a material by surface modification, and a number of elegant and efficient surface treatments have been proposed (*1–5*). Another key property of a surface is its stickiness, or tackiness. A typical example of tackiness is the feeling one has when touching fresh pine resin. This property can be deliberately sought after, such as in adhesive labels, or carefully avoided, as in varnish or paint. In general, a polymer surface has fixed properties—either tacky or nontacky, and hydrophilic or hydrophobic—that vary only slightly with the surrounding conditions such as humidity or temperature. For example, to make a glassy polymer sticky, one has typically to raise the temperature 50° to 60°C above its glass transition temperature. In this context, the design of a system with wetting and adhesive properties that are switchable with temperature over a narrow range of a few degrees presents a formidable challenge. To achieve this goal, we propose here the use of structured polymer films organized at a mesoscopic scale on the order of 10 nanometers.

A material is sticky when the energy required to break its bond with a surface is a thousand times as large as the simple interfacial energy; this extra work comes from the dissipation during the separation process, which involves deformation and friction in the polymer film. Moreover, to achieve a strong bond, a good contact needs to be established between the two surfaces, which requires some degree of softness of the ma-

[1]Unité Mixte de Recherche 167 CNRS/Elf Atochem, [2]Service Agents d'Interfaces, Elf Atochem, 95 rue Danton, 92303 Levallois-Perret, France.

terial. Consequently, a polymer is tacky when it possesses the right balance between softness and ability to dissipate energy. Wettability, on the other hand, is related a priori to a much simpler property of the material: its interfacial energy, which is more readily controlled by the chemical nature and molecular organization of the surface. For example, the use of fluorinated molecules enables one to obtain very oleophobic and hydrophobic coatings.

In order to finely tune the surface properties of a material, we thus propose to use a fluorinated polymer coating that undergoes a first-order phase transition from a highly structured state toward a disorganized state. We show that at the structuring transition, the dissipative properties of the polymer can vary dramatically: the transition from a hard, structured phase to a soft isotropic phase modifies its tackiness. Similarly, we show that the kinetics of spreading of liquids on the surface of a structured polymer is also markedly affected at the phase transition. This behavior is partly due to the change in the surface characteristics of the polymer, but more originally, it is also the result of modifications in the polymer bulk properties at the transition. Hence, by using fluorinated coatings with order-disorder structural transitions, one can tune the adhesive and wettability properties of a material. This opens interesting possibilities for many applications in which surface control is important, in areas as diverse as biotechnology, industrial coatings, and cosmetics. Everyday examples of switchable adhesive applications might include antisoil grips for tennis rackets or golf clubs.

The polymer used is a side-chain liquid crystalline copolymer, obtained by radical copolymerization in butylacetate of 50 mole percent of an acrylate monomer bearing a long perfluoroalkyl side chain (C_2H_4-C_8F_{17}), and 50% of a methacrylate monomer bearing a long alkyl chain ($C_{17}H_{35}$). At room temperature, this copolymer is highly organized: X-ray scattering spectra show several orders of Bragg peak multiple of the wave vector $q = 0.099$ Å^{-1}, indicating the presence of lamellae with a period of 64 Å. Furthermore, the presence of wide-angle Bragg peaks at $2\theta = 17.95°$ and 21.55° indicate that in those lamellae, both the hydrogenated and the fluorinated side chains can crystallize with a characteristic distance of 4.1 and 4.9 Å, respectively. From these data we conclude that the copolymer organizes into a partially crystallized lamellar (or smectic) phase. Moreover, differential scanning calorimetry and x-ray experiments show a wide transition between a mesomorphic and an isotropic phase centered at 35°C (Fig. 1).

The tack properties of the copolymer were studied with a probe tack tester (*6*). The probe is a rectangular quartz prism that enables one to measure, by optical means, the true area of contact between the adhesive and the probe, S, in addition to the adhesive energy. The copolymer was deposited on an aluminum plaque by evaporation from a 20 weight % solution in butylacetate to form a film 100 ± 20 μm thick. The sample was left for 5 min at the desired temperature. The prism was then brought into contact with the coating at a speed of 0.5 mm/s. When the applied force reached 50 N, the motion of the prism was stopped and its position was maintained for 1 s. The probe was eventually pulled up at 0.5 mm/s. By recording the evolution with time of the force F exerted on the probe, we could measure the tack energy per unit surface, defined as the time integral of F during the debonding process multiplied by V/S, where V is the probe speed and S is the true wetted area. In the smectic phase, the energy needed to separate the adhesive from the probe was zero within experimental accuracy, whereas in the isotropic phase, the energy decreased from 50 J/m^2 at 37°C to 14 J/m^2 at 50°C (Fig. 2). These values are typical for a polymer well above its glass transition. For example, the adhesive energy of polyisobutylene at 30°C is 10 J/m^2 (*6*). A remarkable feature of this transition between a nonadhesive and an adhesive regime is that it occurs very abruptly at the smectic-to-isotropic transition. The tack energy increases within a 2°C temperature range, compared with the usual 60° or 70°C for conventional pressure-sensitive adhesives that present a glass transition (*6*). This change in behavior is reminiscent of tack modification at structural transitions in other systems such as alkyl side-chains homopolymers (*7*). Our experiments also show that during the transition, the true area of contact between the adhesive and the probe evolved from less than 10% in the smectic phase to nearly 100% in the isotropic phase (Fig. 2).

Qualitatively, the area of contact A between a coating and a probe after a contact time t depends on the viscoelastic properties of the coating as well as on the roughness of the material. For an elastic and smooth coating of Young's modulus E that faces a hard and rough probe, and for asperities of typical radius of curvature R and a distribution of heights with a characteristic size σ, the relation between A and E can be calculated in the framework of a Hertz contact (*8*): $A \approx (F/E)(R/\sigma)^{1/2}$, where F is the load applied on the probe. For a given roughness, one thus expects the wetted area to differ substantially in the isotropic phase, where E is typically on the order of 10^5 Pa, and in the smectic phase, where it is rather on the order of 10^8 Pa (*9*, *10*). If one assumes, for a 1-cm^2 surface area, a "typical" roughness $(R/\sigma)^{-1/2}$ on the order of 0.1 (*8*), one expects a wetted area of 100% in the isotropic phase for a force as low as 1 N, whereas in the smectic phase, the experimental 50 N applied would create a contact area of only 5% of the total surface. This result is in good agreement with the experiments performed for different contact forces.

The sharp increase at the transition of the adhesion energy, which has been normalized by the true contact area, is the signature of an abrupt change of the dissipative ability of the material during the debonding process. The available experimental data, in slightly different systems that exhibit smectic A phases, indeed show a large difference in the rheological properties of isotropic and smectic phases (*9*, *10*). In the isotropic range, the decrease of the adhesion energy reflects the decrease of the viscoelastic dissipation when we further increase temperature.

Wetting and dewetting phenomena are another way of probing both the interfacial and viscoelastic properties of a material. Indeed, experimental and theoretical studies (*11*–*16*)

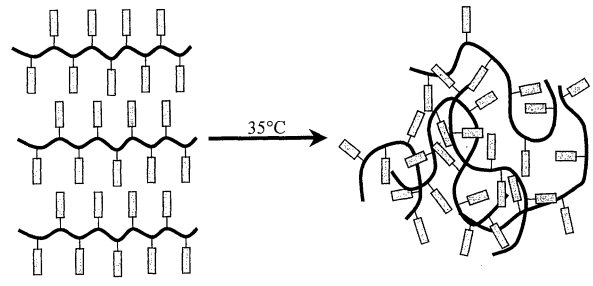

Fig. 1. Schematic representation of the transition between the smectic and the isotropic phase.

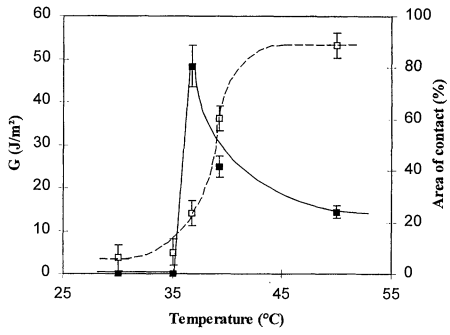

Fig. 2. Tack (■) and percentage of the probe wet by the film (□) for the fluorinated copolymer as a function of temperature. The lines serve as a guide to the eye. The smectic-to-isotropic transition is located at 35°C.

have shown that, on hard substrates, the dynamics of wetting and dewetting is controlled by the interfacial properties of the substrate, whereas on a deformable material, it tends to be controlled by the viscoelastic dissipation in the material. In the latter case, because of the unbalanced vertical component of the surface tension, a wetting ridge of approximate size γ_1/E appears, where γ_1 is the liquid surface tension. The energy dissipated by the displacement of this ridge can be much more important than the viscous losses in the liquid wedge. This effect leads to a "viscoelastic braking" (*15*) of the droplet contact line.

We studied the temperature dependance of the dewetting velocity of a liquid, chosen for its high viscosity, on the fluorinated smectic copolymer. A thin metastable (*17*) film (~100 μm thick) of a hydroxy-terminated polybutadiene (pBdOH) is forced onto a copolymer film (~30 μm thick) that was deposited on a glass plate in the heating stage. After being thermally equilibrated for 5 min at temperatures ranging from 20° to 40°C, the liquid film was destabilized with a pin and a dry patch opened. The evolution of this dry hole with time was followed under a low-magnification microscope and recorded with a video camera. The opening hole was surrounded by a rim that collected the liquid (Fig. 3). We measured independently the viscosity η_1, the surface tension γ_1, and both the advancing and receding contact angle of pBdOH versus temperature, because they are key parameters to interpreting the dewetting velocity. The temperature dependence of the contact angles, measured by the Wilhelmy plate method, is shown in Fig. 4.

Over this entire temperature range, the radius r of the opening hole increased linearly with time with a well-defined dewetting velocity dr/dt. Its evolution with temperature (Fig. 5) showed two regimes: The velocity in the smectic phase, which increases slowly with temperature up to a value of 110 μm/s at 27°C, drops abruptly to 5 μm/s at the isotropic transition. This effect is seen on Fig. 3, which shows the opening of a dry patch at 27° and 32°C for the same intervals of time. When the temperature was raised even further in the isotropic phase, the dewetting velocity increased slightly again.

We first interpret the observations in the smectic phase. As explained above, the smectic is a "hard" material, which behaves as a solid substrate. In this case, it is predicted (*18*) that the dewetting velocity of the viscous liquid is constant and scales as $(\gamma_1/\eta_1)\theta_e^3$ where θ_e is the contact angle between the liquid and the substrate. Although this theory is expected to be valid only for small contact angles and small hysteresis, which is obviously not the case in our study, our experimental data are well fitted with this theoretical expression if we take $\theta_e = (\theta_a + \theta_r)/2$, where θ_a and θ_r denote the advancing and receding contact angles. A prefactor can be extracted, which is expressed as the logarithm of the ratio of two lengths (*19*): a macroscopic cutoff, taken as the size of the rim section, and a molecular size. In the case of our experiment, the fit gives a factor of 15 ± 0.5, which is in agreement with the values predicted and those experimentally found (*20*) on the order of 10.

Two effects are likely to contribute to the sharp drop in the dewetting velocity at the transition: a surface modification and a change of the bulk properties of the material. Below we attempt a rough evaluation of their respective contributions.

The data of Fig. 4 show that there is indeed a large variation of the contact angles at the transition temperature. The larger hysteresis $\Delta\theta = \theta_a - \theta_r$ in the isotropic phase can have different sources, such as a difference in roughnesses, a swelling of the coating, or surface reconstruction. This last phenomenon, corresponding to the reorientation of molecules at the surface so as to minimize their interfacial energy with the surrounding medium (*21*, *22*), is the one most likely to occur in our systems. From a thermodynamic point of view, the moieties oriented toward the surface should be fluorinated if the copolymer is exposed to air (when measuring θ_a) and hydrogenated if the surface is exposed to pBdOH (when measuring θ_r). However, one should consider kinetic factors such as the ability of the molecules to reorganize within the experimental time scale. Because the mobility is much smaller in the smectic phase, there is no or little reconstruction in this phase as compared with the isotropic one. The drop in velocity that should result from the modification of the equilibrium contact angle, $\theta_e = (\theta_a + \theta_r)/2$, from 85° in the smectic phase to 75° in the isotropic one, would account for a decrease of V by a factor 1.4 ± 0.2, significantly smaller than the factor of 20 experimentally observed.

Hence, consideration of only the surface properties is insufficient to account for the observed transition in dewetting velocity. A possible explanation for this drop of V could be a change in the viscoelastic properties of the material. Indeed, the modulus of the polymer is far lower in the isotropic than in the smectic phase; consequently, the deformation of the substrate has to be taken into account in the isotropic phase as it becomes important: $\gamma_1/E \sim 0.4$ μm (with the measured $\gamma_1 = 40$ mN/m) and, as explained above, the motion of the deformed region causes the extra dissipation responsible

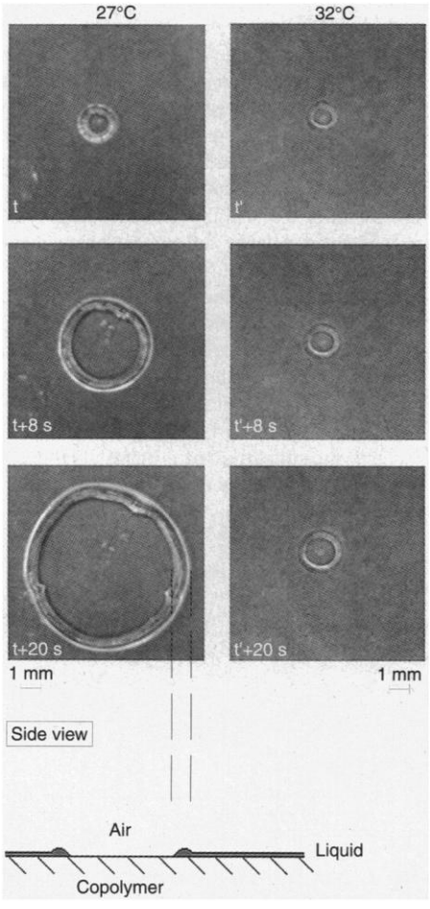

Fig. 3. Opening of a dry hole above and below the phase transition for three different times separated by the same time interval.

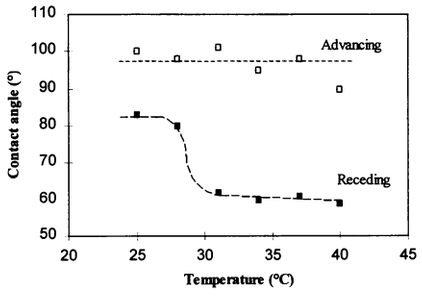

Fig. 4. Advancing and receding contact angles of pBdOH on the copolymer as a function of the temperature.

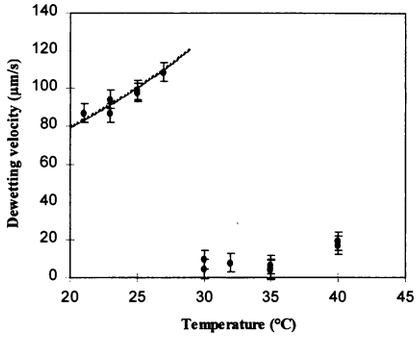

Fig. 5. Dewetting velocity of pBdOH on the fluorinated copolymer as a function of the temperature. The dashed line represents a theoretical fit (values given in the text).

for the drop slowing down. A detailed calculation of the velocity drop would require the knowledge of the viscoelastic properties of the liquid crystalline polymer, which are quite complex. Nevertheless, if we approximate the polymer by a visquous liquid of typical viscosity $\eta = 10^4$ Pa·s, we obtain (*16*) a velocity on the order of 5 μm/s, in agreement with the experimental results.

We have performed tack and dewetting experiments on a smectic polymer liquid crystal around the lamellar-to-isotropic phase transition. Specific behaviors that reflect the complex structure of the system are exhibited. Through the side-chain ordering, the smectic structure brings hardness and nonwettability. In contrast, in the isotropic phase, the presence of the backbone, which connects the side chains together, allows for a strong dissipation that leads to both a tacky behavior and an ability to slow down the dynamics of wetting. On each side of the phase transition, a different aspect of the hybrid macromolecule becomes predominant and imprints its behavior onto the system. This effect can be used to design versatile materials with highly flexible properties that vary with temperature. Moreover, the transition temperature can be tuned by changing the copolymer composition, which may be useful for different types of applications. Finally, the reversibility of the structural transitions and of the resulting properties with temperature is another interesting feature of the system.

References and Notes

1. I. Langmuir, *Trans. Faraday Soc.* **15** (no. 3), 62 (1920).
2. A. G. Pittman, *Fluoropolymers*, L. A. Wall, (Wiley, New York, 1972), vol. 25.
3. R. Maoz and J. Sagiv, *J. Colloid Interface Sci.* **100**, 465 (1984).
4. C. D. Bain, J. Evall, G. M. Whitesides, *J. Am. Chem. Soc.* **111**, 7155 (1989).
5. P. Mansky, Y. Liu, E. Huang, T. P. Russell, C. Hawker, *Science* **275**, 1458 (1997).
6. A. Zosel, *Colloid Polym. Sci.* **263**, 541 (1985).
7. R. Clarke, A. Larson, E. E. Schmidt, S. P. Bitler, *Adhesive Age* (September 1993), p. 39.
8. C. Creton and L. Leibler, *J. Polym. Sci. Polym. Phys.* **34**, 545 (1996).
9. B. H. Rottink, K. te Nijenhuis, R. Addink, W. J. Mijs, *Polym. Bull.* **31**, 221 (1993).
10. T. Yamaguchi, T. Asada, N. Koide, *Mol. Cryst. Liq. Cryst.* **214**, 1 (1992).
11. P. G. de Gennes, *Rev. Mod. Phys.* **57**, 827 (1985).
12. A. Carre, J. C. Gastel, M. E. R. Shanahan, *Nature* **379**, 432 (1996).
13. M. E. R. Shanahan and A. Carre, *Langmuir* **11**, 1396 (1995).
14. ———, *J. Adhesion* **57**, 179 (1996).
15. M. E. R. Shanahan, *J. Phys. D* **21**, 981 (1988).
16. D. Long, A. Ajdari, L. Leibler, *Langmuir* **12**, 21, 5221 (1996).
17. F. Brochard-Wyart, F. Rondelez, C. Redon, *C.R. Acad. Sci. Paris Ser. II*, **306**, 1143 (1988).
18. F. Brochard-Wyart, J. M. di Meglio, D. Quéré, *ibid.* **304**, 553 (1987).
19. C. Andrieu, C. Sykes, F. Brochard, *J. Adhesion* **58**, 15 (1996).
20. C. Redon, F. Brochard-Wyart, F. Rondelez, *Phys. Rev. Lett.* **66**, 6 (1991).
21. T. Kasemura, S. Takahashi, N. Nakane, T. Maegawa, *Polymer* **37**, 16, 3659 (1996).
22. H. S. Van Damme, A. H. Hogt, J. Feijen, *J. Colloid Interface Sci.* **114**, 1, 167 (1986).

23. We thank A. C. Aubert la Fayette for synthesis of the copolymers. We are indebted to S. Girault for the structural investigation, C. Gay for fruitful discussion, and M. Bourrel and P. Tordjeman for the use of their probe tack tester.

12 March 1999; accepted 29 June 1999

Chemical "Double Slits": Dynamical Interference of Photodissociation Pathways in Water

R. N. Dixon,[1]* D. W. Hwang,[2] X. F. Yang,[2]† S. Harich,[2] J. J. Lin,[2] X. Yang[2]

Photodissociation of water at a wavelength of 121.6 nanometers has been investigated by using the H-atom Rydberg tagging technique. A striking even-odd intensity oscillation was observed in the OH(X) product rotational distribution. Model calculations attribute this oscillation to an unusual dynamical interference brought about by two dissociation pathways that pass through dissimilar conical intersections of potential energy surfaces, but result in the same products. The interference pattern and the OH product rotational distribution are sensitive to the positions and energies of the conical intersections, one with the atoms collinear as H–OH and the other as H–HO. An accurate simulation of the observations would provide a detailed test of global H_2O potential energy surfaces for the three ($\tilde{X}/\tilde{A}/\tilde{B}$) contributing states. The interference observed from the two conical intersection pathways provides a chemical analog of Young's well-known double-slit experiment.

The photodissociation of water, a unimolecular process, can be studied from first principles, and extensive experimental and theoretical studies have been performed on this system during the last few decades. Excitation in its longest wavelength ultraviolet absorption band between 150 and 200 nm populates the lowest excited ($\tilde{A}$) state. Dissociation from this state takes place on a single potential energy surface and forms an H atom and a ground-state OH ($X^2\Pi$) molecular product (*1*).

In contrast, three electronic states of the water molecule are implicated in its photochemistry at the Lyman-α wavelength (λ = 121.6 nm). The initial excitation is to the third ($\tilde{B}$) state, which correlates adiabatically with an H atom and an excited electronic state of the OH partner ($A^2\Sigma^+$). However, the dominant dissociation leads to an H atom plus a ground-state OH molecule, which is brought about by a nonadiabatic crossing from the $\tilde{B}$ state to the potential energy surfaces of either the $\tilde{A}$ state or the ground ($\tilde{X}$) state of water. Although extensive information on the photodissociation through the $\tilde{B}$ state has been obtained through these studies, a quantitative picture is still lacking.

Conical intersections of potential energy surfaces play an important role in the dynamics of many excited electronic states. The extremely high rotational excitation of the OH product that arises from excitation to the $\tilde{B}$ state has been attributed to such an intersection. Dynamical calculations have shown that this high average rotational angular momentum results from a high torque acting in the vicinity of a conical intersection at a linear (H-O-H) geometry of the excited and ground-state potential energy surfaces of H_2O (*2*). This conical intersection arises because, for a linear approach of H to OH, a repulsive potential curve from H + OH($X^2\Pi$) can cross an attractive potential curve from H + OH($A^2\Sigma^+$), whereas there is an avoided crossing of these curves in the lower symmetry of a bent geometry.

Besides the conical intersection for the H-O-H geometry, there is second symmetry–determined conical intersection on the $\tilde{B}$ state surface for the linear O-H-H geometry. The importance of this second intersection in the O(^{1}D, ^{3}P) + H_2 reaction system has been

[1]School of Chemistry, University of Bristol, Bristol BS8 1TS, UK. [2]Institute of Atomic and Molecular Sciences, Academia Sinica, Taipei, Taiwan 106, R.O.C.

*To whom correspondence should be addressed. E-mail: r.n.dixon@bristol.ac.uk

†Permanent address: Laboratory of Plasma Physical Chemistry, Dalian University of Technology, Dalian 116024, China.